Upscale Synthesis of Magnetic Mesoporous Silica Nanoparticles and Application to Metal Ion Separation, Nanosafety Evaluation

Mathilde Ménard *, Lamiaa M.A. Ali *, Ani Vardanyan *, Clarence Charnay, Laurence Raehm, Frédérique Cunin, Aurélie Bessière, Erwan Oliviero, Theodossis A. Theodossiou, Gulaim A. Seisenbaeva, Magali Gary-Bobo, Jean-Olivier Durand

Posted Date: 23 October 2023

doi: 10.20944/preprints202310.1429.v1

Keywords: Magnetic Mesoporous Nanoparticles; Up scaled synthesis. DTPA; Metal ion separation, Toxicity

Article

Upscale Synthesis of Magnetic Mesoporous Silica Nanoparticles and Application to Metal Ion Separation, Nanosafety Evaluation

Mathilde Ménard [1,*], Lamiaa M.A. Ali [2,*], Ani Vardanyan [3,*], Clarence Charnay [1], Laurence Raehm [1], Frédérique Cunin [1], Aurélie Bessière [1], Erwan Oliviero [1] Theodossis Theodossiou, [4] Gulaim Seisenbaeva, [3] Magali Gary-Bobo, [2] and Jean-Olivier Durand [1]

[1] ICGM, Univ Montpellier, CNRS, ENSCM; Montpellier, France. mathilde.menard@umontpellier.fr, (M.M.), clarence.charnay@umontpellier.fr (C.C.), laurence.raehm@umontpellier.fr (L.R.). frederique.cunin@enscm.fr (F.C.), aurelie.bessiere@umontpellier.fr (A.B.), erwan.oliviero@umontpellier.fr (E.O.)°, jean-olivier.durand@umontpellier.fr (J.-O.D.)

[2] IBMM, Univ Montpellier, CNRS, ENSCM; Montpellier, France. miss_limo@yahoo.com (L.M.A.A.), magali.gary-bobo@inserm.fr (M.G.)

[3] Department of Molecular Sciences, Swedish University of Agricultural Sciences, 750 07 Uppsala, Sweden, ani.vardanyan@slu.se (A.V.), Gulaim.Seisenbaeva@slu.se (G.S.)

[4] Department of Radiation Biology, Institute for Cancer Research, Radium Hospital, Oslo University Hospital, Montebello 0379 Oslo, Norway, Theodossis.Theodossiou@rr-research.no (T.T.)

* Correspondence: mathilde.menard@umontpellier.fr, (M.M.), miss_limo@yahoo.com (L.M.A.A.), ani.vardanyan@slu.se (A.V.)

Abstract: (1) Background: The synthesis of core-shell magnetic mesoporous nanoparticles (MMSN) from phase transfer process is usually performed at 100-250 mg scale. At the gram scale, nanoparticles without core or with multicore systems are observed. (2) Methods: Iron oxide core nanoparticles (IO) were synthesized through thermal decomposition procedure of -FeO in oleic acid. Phase transfer from chloroform to water was then performed in order to wrap IO with mesoporous silica shell through the sol-gel procedure. MMSN were then functionalized with DTPA, and used for the separation of metal ions. Their toxicity was evaluated (3) Results: The phase transfer procedure was crucial to obtained MMSN at large scale. Three synthesis parameters were rigorously controlled: temperature, time and glassware. Homogeneous dispersion of MMSN at the gram scale was successfully obtained. After functionalization with DTPA, the MMSN-DTPA were shown to have a strong affinity for Ni ions. Furthermore toxicity was evaluated in cells, zebrafish and through seahorse metabolic assays, and the nanoparticles were found nontoxic. (4) Conclusions: We developed a method of preparation of MMSN at the gram scale. After functionalization with DTPA, the nanoparticles were efficient in metal ion removal and separation, furthermore, no toxicity was noticed up to 125 μg.mL^{-1} in zebrafish.

Keywords: magnetic mesoporous nanoparticles; up scaled synthesis; DTPA; metal ion separation; toxicity

1. Introduction

The use of core-shell Magnetic Mesoporous Silica Nanoparticles (MMSN) has grown a lot over the last decade. Many different applications were described such their use as as theranostic agents for magnetic resonance imaging, and drug delivery, for cancer applications[1–3], sensor agents for sensitive detections[4,5], or extracting agents for removal of heavy metal ions[6,7] and rare earth elements.[8] The field of MMSN and their applications have been comprehensively discussed and reviewed.[9–19] Two groups independently reported the first preparation of MMSN in 2008. [20,21] Zink's group encapsulated iron oxide nanoparticle core of 20 nm diameter in MSN of 100-200 nm diameters. The preparation consisted of first the thermal decomposition of iron-oleate complexes at

 doi:10.20944/preprints202310.1429.v1

320°C in octadecene-oleic acid to lead to the nanoparticle core. Then the iron-oxide nanocrystals coated with oleic acid were transferred in aqueous solution with cetyltrimethylammonium bromide (CTAB) by dispersion of the nanocrystals in chloroform and evaporation of the volatiles. Subsequent hydrolysis-polycondensation of tetraethoxysilane in the presence of CTAB led to MMSN. Hyeon's group essentially used the same procedure for the synthesis of monodisperse MMSN of different diameters (45-105 nm) with cores of 15 nm. 22 nm core was also used. Note that MMSN synthesis is not an easy task[22] and is usually performed at 150-250 mg scale, in order to obtain homogeneous monodisperse, well dispersed core–shell nanoparticles. The preparation often leads to a mixture of nanoparticles with multi Fe_3O_4 cores per particle or mesoporous silica nanoparticles without core, particularly when upscaling is carried out. In the course of our work on MMSN for metal removal, we present here a detailed procedure in order to synthesize monodisperse MMSN of 100 nm diameter, with 18 nm magnetic core diameter, at the gram scale. MMSN were then functionalized with diethyl triamino pentacetic acid (DTPA) for the extraction and separation Ni(II), Co(II), Sm(III), and Nd(III) ions. The non toxicity of MMSN was evaluated in cells, zebrafish embryos, and with seahorse metabolic assays.

2. Results and discussion

2.1. Preparation of MMSN and MMSN-DTPA.

The principle of the synthesis and functionalization of MMSN is presented in Figure 1.

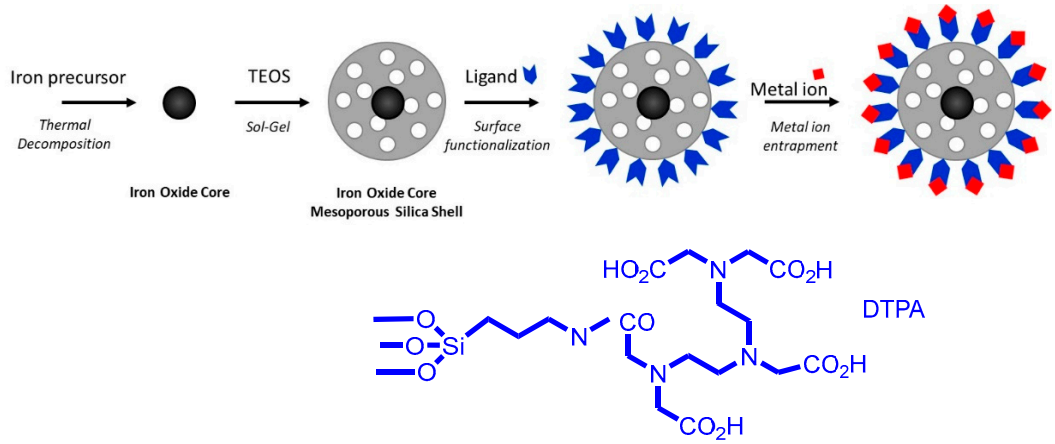

Figure 1. Preparation of MMSN functionalized with DTPA.

The synthesis of core-shell nanoparticles made of an iron oxide core and a porous silica shell was deeply investigated and described this last decade. Indeed, researchers were able to precisely tune the size of the shell by variating the Fe/surfactant ratio.[21]. Nevertheless, to the best of our knowledge, the syntheses of homogeneous core-shell nanoparticles never exceed the 100 mg scale. Thus, the scale-up of these objects to the gram scale remains challenging.

We first investigated the scale-up experiment by increasing homogeneously all quantities (TEOS, surfactant, iron oxide core, solvents) to reach the gram scale. This method only led to a non-negligible amount of unwanted "no-core" porous silica particles mixed with the wanted core-shell particles, **Figure 2 (a)**. Size analysis made by measuring more than 400 NPs from TEM images showed that the number of "no-core" NPs is close to the number of core-shell NPs (48% *versus* 52% respectively, **Figure 2 (b)**).

Preprints (www.preprints.org) | NOT PEER-REVIEWED | Posted: 23 October 2023 doi:10.20944/preprints202310.1429.v1

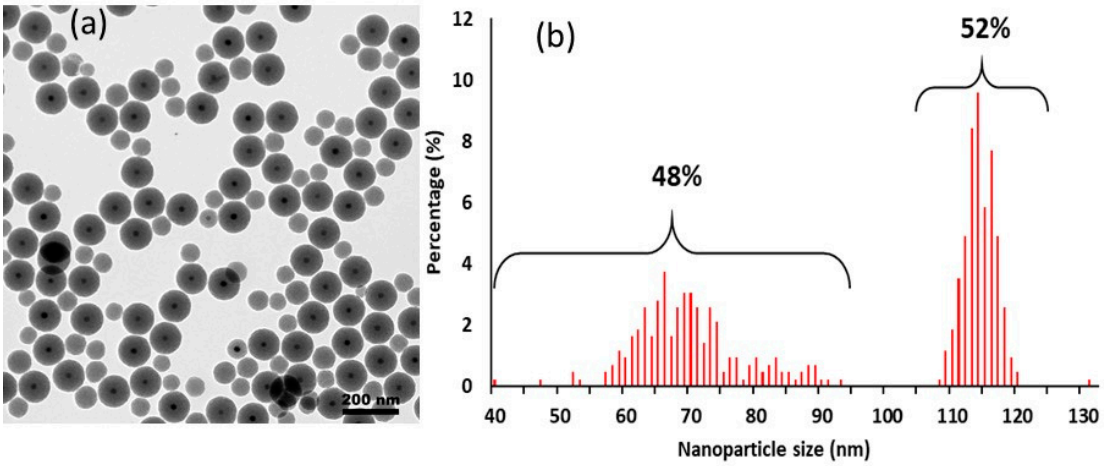

Figure 2. Morphological effect of an excess of CTAB on scale-up protocol: **(a)** Brigh-field TEM image (scale bar 200 nm) and **(b)** size analysis (on 428 NPs from TEM images).

As an excess of surfactant which can act as soft template to initiate the sol-gel reaction could lead to the presence of "no-core" porous silica particles, the CTAB amount was decreased from 25% compared to the 100 mg protocol. This simple protocol modification allowed to obtain a gram of monodispersed core-shell NPs but unfortunately this was not always reproducible which implies that other key parameters had to be considered. Indeed, although the presence of "no-core" NPs was not noticed, "multiple-cores" NPs were observed in some experiments (**Figure 3**).

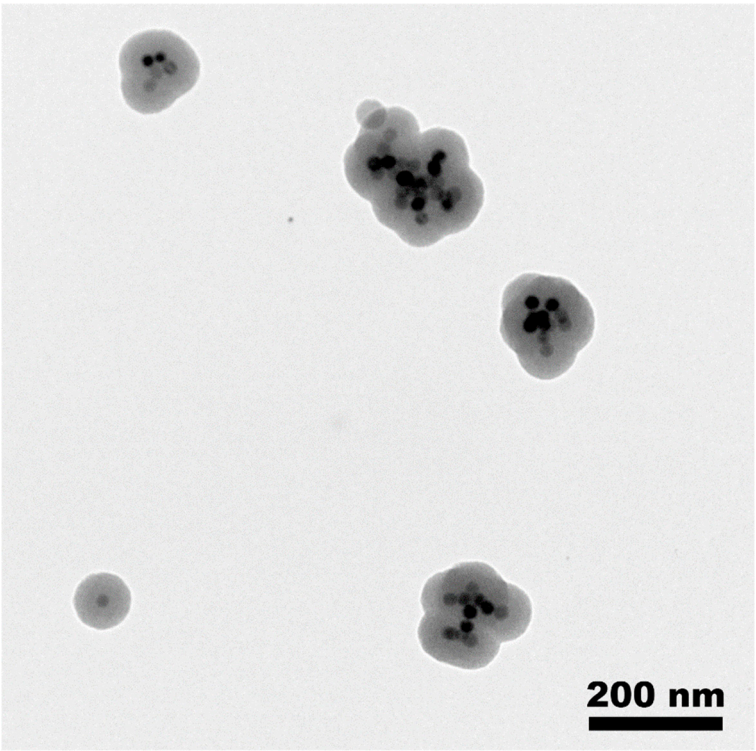

Figure 3. Bright-field TEM image showing the morphological effect of a fail in phase transfer (Scale bar 200 nm).

Two key parameters which can lead to this result were identified. First: the stability of the core material. Indeed, **iron oxide (**IO**)** cores which are not perfectly dispersed and stabilized in chloroform will aggregate and form "multiple core"-shell structures. These dispersion issues were often due to extensive washing steps after thermal decomposition that desorb oleic acid from IO surface. This can be easily verified by DLS measurements on IO cores before the sol-gel reaction step or by observing

 doi:10.20944/preprints202310.1429.v1

the sedimentation of the sample when stored. The second parameter is harder to control: the phase transfer of IO cores from chloroform to aqueous solution. This phase transfer, widely described in literature [23] is based on the formation of water-soluble nano-micelles driven by the hydrophobic **V**an der Waals interactions between the alkyl chains of the surfactant and the oil-stabilizing ligand forming an **i**nterdigitated bilayer structure around the IO core. Complete removal of chloroform during the phase transfer is also necessary to obtain water stable nano-micelles without clustering. Thus, controlling th**ese** key synthesis step**s** is important to succeed in the scale-up. Three synthesis parameters were controlled: temperature, time and glassware. Before the addition of IO NPs**,** the solution containing dissolved CTAB had to be cooled down to 40°C to avoid the instant evaporation of chloroform. To ensure a good oil/water emulsion the mixture was placed under stirring without heating for 30 min. Then to secure the phase transfer of IO NPs through complete chloroform evaporation and proper Van der Waals interactions between oleic acid and CTAB, the temperature was increased to 70°C and the mixture was kept at this temperature under stirring for additional 40 min. Finally, to achieve a better stirring to foster oil/water emulsion and a higher liquid/air interface to facilitate chloroform evaporation, the syntheses were performed in large bottom **b**eaker or Erlenmeyer flasks. The rest of the protocol, which consisted of the sol-gel reaction (dilution in water, addition of a base, TEOS and EtOAc and aging at 70°C for 3h) was kept identical as previously developed. Following this method homogeneous monodispersed core-shell nanoparticles were obtained, **Figure 4**. These NPs were then used for the surface grafting of DTPA.

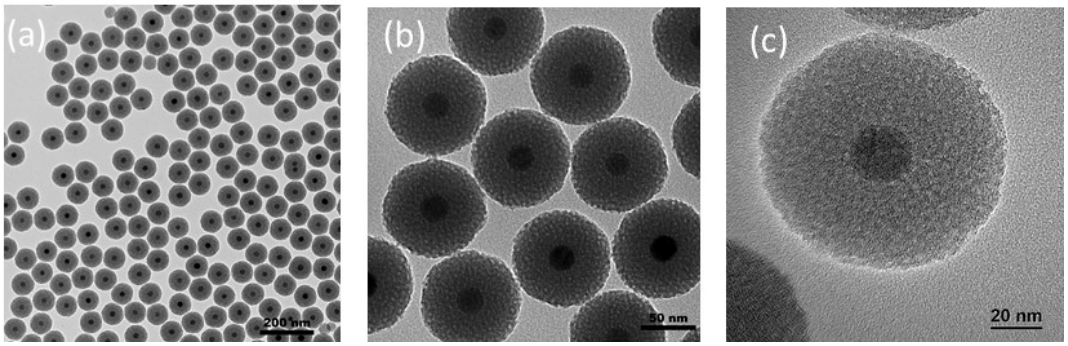

Figure 4. Bright field TEM images of MMSN obtained through the 1g scale protocol. (a) 120 kV TEM. (b,c) 200 kV HRTEM at two different magnifications.

To assess the success of DTPA grafting onto MMSN comparative FTIR, TGA and Zeta analyses were performed.

The apparition on FTIR spectra of $\nu_{N\text{-}C}$ at 1395 cm^{-1} and $\nu_{C=O}$ at 1650 cm^{-1} demonstrated the grafting of DTPA (**Figure 5**). This was also confirmed by a drop in Zeta potential values compared to raw MMSN due to the surface modification (**Figure 6**). Finally, TGA analyses showed a final weight-loss difference of 20.5% which corresponds to a grafting of 0.6 mmol of DTPA per gram of MMSN (**Figure 7**).

Preprints (www.preprints.org) | NOT PEER-REVIEWED | Posted: 23 October 2023 doi:10.20944/preprints202310.1429.v1

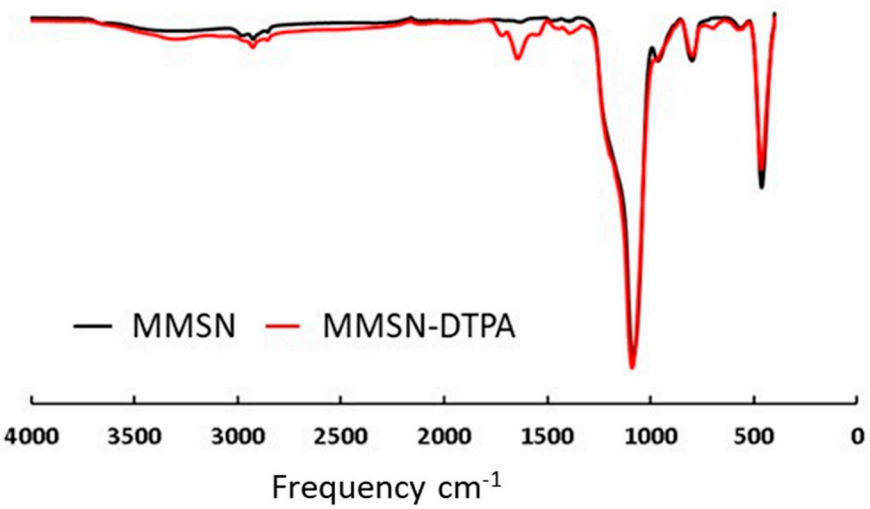

Figure 5. FTIR of MMSN and MMSN-DTPA showing functionalisation.

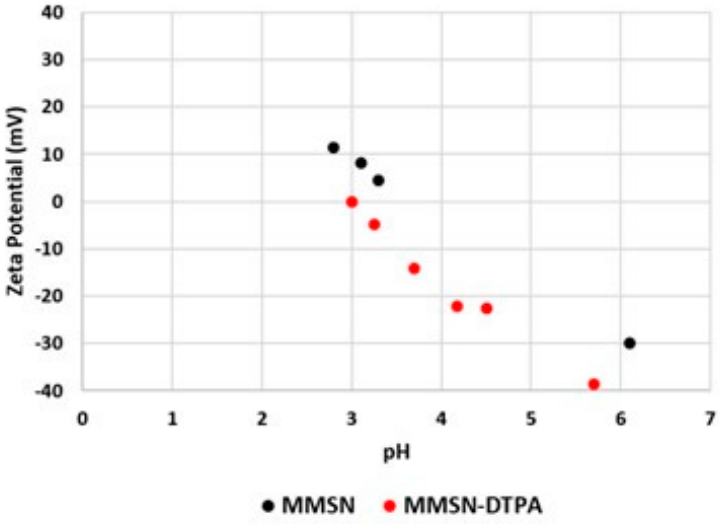

Figure 6. Zeta potential of MMSN and MMSN-DTPA.

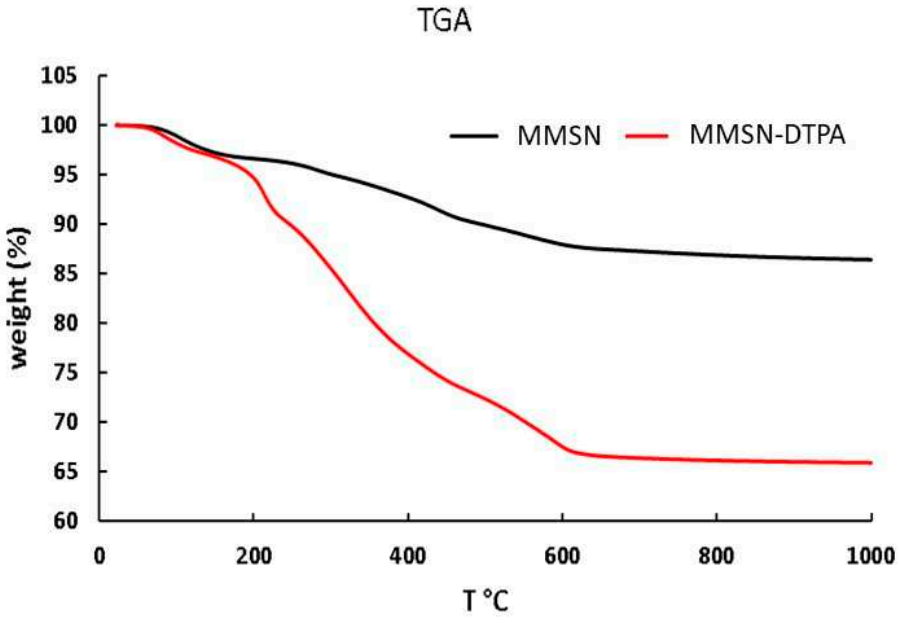

Preprints (www.preprints.org) | NOT PEER-REVIEWED | Posted: 23 October 2023 doi:10.20944/preprints202310.1429.v1

Figure 7. TGA of MMSN and MMSN-DTPA showing the functionalization.

2.2. Adsorption of heavy metals using MMSN and MMSN-DTPA.

Raw **MMSN** showed considerably lower capacity for both heavy metals (1.00 mmol/g) and appreciably less for the REE (0.88 and 0.85 mmol/g for Nd and Sm respectively) whereas with DTPA surface modification almost doubled the adsorption capacity (**Table 1**).

Table 1. Average maximum adsorption capacity for each magnetic nanoadsorbent and heavy metal (mmol/g).

Sample	Ni	Co	Nd	Sm
MMSN	1.00	1.00	0.88	0.85
MMSN-DTPA	2.16	1.44	2.00	1.66

Adsorption isotherms of metal cations were best fit with Langmuir curves, having higher correlation coefficients compared to Freundlich model (**Figure 8)**

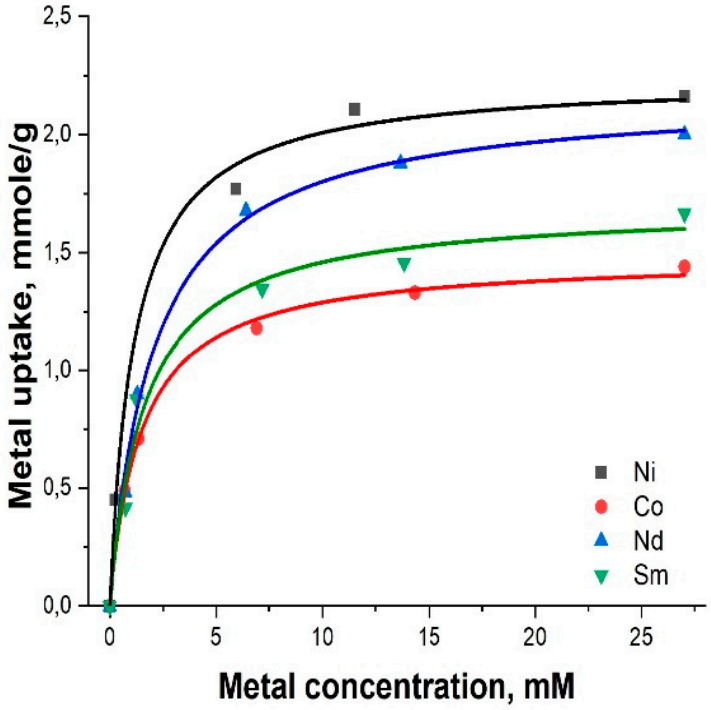

Figure 8. Langmuir isotherms for MMSN-DTPA NPs.

For kinetic test results showed fast uptake at the first 1-2 hours of metal interaction with MMSN-DTPA, reaching over 70% of the total capacity. Slower uptake was observed after these 2 hours and the equilibrium was reached after 5-6 hours (**Figure 9**).

Preprints (www.preprints.org) | NOT PEER-REVIEWED | Posted: 23 October 2023 doi:10.20944/preprints202310.1429.v1

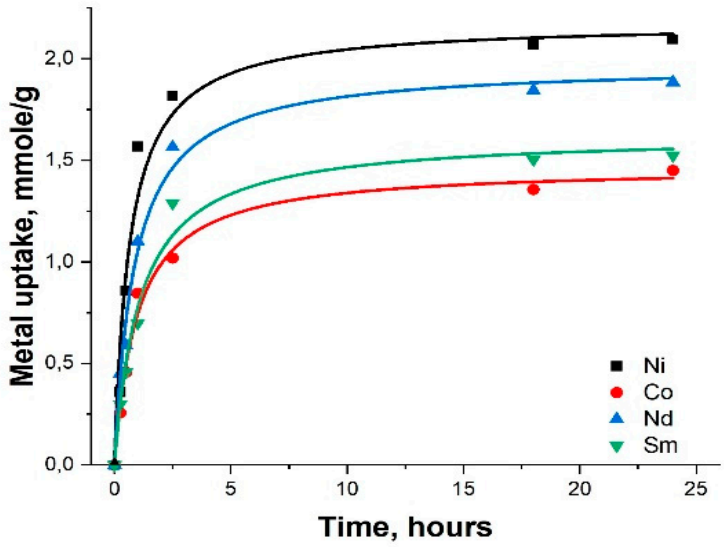

Figure 9. Adsorption kinetics of heavy metals with MMSN-DTPA.

Selectivity tests revealed considerable difference in metal uptake in pairs, showing appreciable preference of MMSN-DTPA for Ni as opposed to Nd, and Ni rather than Co, while lower selectivity was observed in the Co-Sm pair in favour to Sm (see **Table 2**).

Table 2. Selectivity of MMSN and MMSN-DTPA in relation to separation of cations.

Sample	Ni:Nd	Co:Sm	Ni:Co
MMSN			**1:1**
MMSN-DTPA	**12:1**	**1:2.4**	**9.4:1**

2.3. Nanosafety

First the nanosafety of MMSN and MMSN-DTPA was investigated by *in vitro* cell viability studies in healthy human dermal fibroblasts. After 3 days of incubation with varying concentrations of MMSN or MMSN-DTPA, a similar cytotoxic response was observed for both nanoparticles (**Figure 10**). The cell viability results showed the classical sigmoidal dose-response curves when plotted versus the logarithmic function of nanoparticle concentration (**Figure 10**). Calculation of the LC_{50} values for both nanoparticles yielded the same value of 32 μg mL^{-1} for both. These results indicated that the surface modification does not have a crucial impact on the nanoparticles cytotoxic behaviour in these experimental conditions.

Preprints (www.preprints.org) | NOT PEER-REVIEWED | Posted: 23 October 2023 doi:10.20944/preprints202310.1429.v1

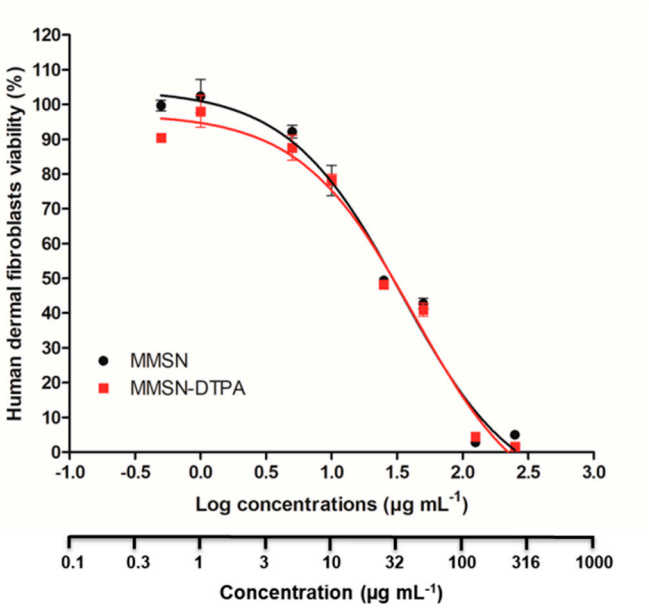

Figure 10. Dose-response curve of healthy human dermal fibroblasts treated with different concentrations of MMSN or MMSN-DTPA for 72 h. Data are presented as mean ± SEM of three independent experiments.

The toxic effect of MMSN or MMSN-DTPA on zebrafish embryos development was evaluated as shown in **Figure 11**. Embryos at 5 hours post fertilization (hpf) were exposed to water containing different concentrations of nanoparticles, the mortality and the viability of embryos were observed until 80 hpf. The results showed that no significant toxicity (death) was observed for MMSN, even at 250 µg mL^{-1}, in comparison to control, whereas the toxicity was significant with DTPA coating at this concentration, reaching 65 ± 14 % of mortality at 80 hpf (**Figure in 11**). Nevertheless, MMSN-DTPA did not have a significant toxicity at lower concentrations.

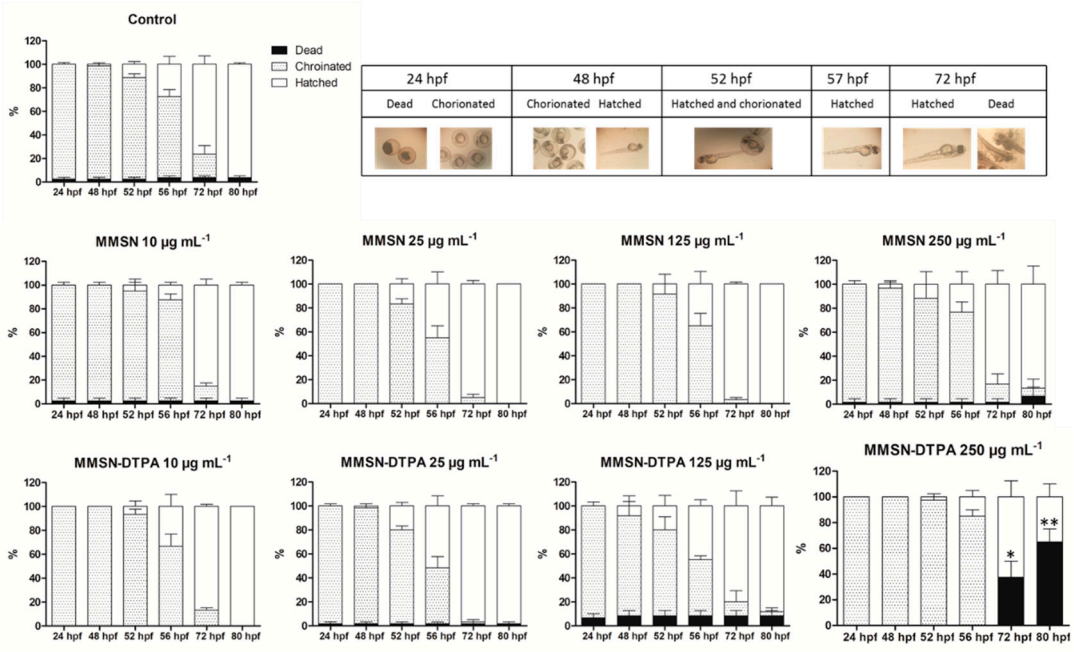

Figure 11. Toxicological study of different concentrations of MMSN or MMSN-DTPA on zebrafish embryos development at different time points. Data are presented as mean ± SEM of three independent experiments. * Dead embryos in the test groups are statistically different from dead embryos in control, the level of significance was defined * $p < 0.05$, and ** $p < 0.005$.

 doi:10.20944/preprints202310.1429.v1

The results of the Seahorse metabolic measurements are presented in **Figure 12**. The oxygen consumption rate (OCR) measurements appear in **Figure 12 (a)** while the extracellular acidification rate (ECAR) measurements are shown in **Figure12 (b)**. From the data presented in **Figure 12 (a)** we can observe that the T47D cells are less respiratory than the SKOV3 cells. In addition T47d cells exhibited equal basal and maximal respiration rates, while for SKOV3 cells their maximal respiration (FCCP-uncoupled mitochondria), was approximately double their basal respiration. In T47D cells there was a marginally significant reduction in both basal and maximal respiration upon incubation with either 5 or 50 μg/mL of MMSN nanoparticles, with no notable concentration dependence. Nevertheless, following incubation with MMSN-DTPA nanoparticles there was a significant reduction of the respiration rates (both basal and maximal) by approximately 50%. Again this drop seemed to be similar for 5 and 50 μg/mL MMSN-DTPA concentrations. In the case of the SKOV3 cells, the basal and maximal respiration rates (as seen through the OCR) did not seem to change after incubation with 5 μg/mL of MMSN, but there was an increase in the basal respiration for incubation with 50 μg/mL of the order of ~25%, while a similar response was observed following incubation with either 5 or 50 μg/mL of MMSN-DTPA. A similar trend was followed by the maximal respiration of SKOV3, however, in this case the increase was of the order of ~40-50%.

With regard to ECAR, the two cell lines exhibited similar basal glycolysis rates, however upon addition of oligomycin, T47D did not significantly increase their glycolysis rate while in the case of SKOV3 cells, the glycolysis rate almost doubled, upon the oligomycin stimulus. Notably, oligomycin inhibits the respiratory ATP production and hence cells, increase their glycolytic activity, to compensate for the ATP loss. With respect to T47D cells there was no notable change in their ECAR and hence glycolysis rate upon incubation with the nanoparticles with or without DTPA, and also regardless of the incubation concentration. SKOV3 cells however reacted by approximately doubling their glycolysis rates following incubation with 5 μg/mL of either MMSN or MMSN-DTPA nanoparticles. Incubation with 50 μg/mL of either nanoparticle moiety, however, caused a reduction of the glycolysis rate by ~25% . The maximal glycolytic capacity of SKOV3 cells also followed a similar trend.

In general the SKOV 3 cells are more metabolically active than T47D cells and are also more reactive to stress stimuli both with regard to raising their respiration and glycolysis rate. In addition, the two cell lines responded differently to incubation with the nanoparticles under investigation. The T47D respiration was impaired following incubation with the MMSN-DTPA nanoparticles. This impairment was not concentration dependent, at least in the range 5-50 μg/mL, and the cell line was not able to compensate this by increasing the glycolysis rate, since the T47D cells seem to perform basal glycolysis at their highest possible capacity. The respiratory and glycolytic increases in SKOV 3 cells following incubation with the nanoparticles, indicates an increased requirement for energy following the insult, which however did not reach their maximal glycolytic capacity (as registered by the addition of oligomycin). However in the case of incubation of SKOV 3 cells with 50 μg/mL regardless of nanoparticle moiety, the glycolytic rate droped back down in comparison to that at 5 μg/mL of nanoparticles, which indicates a probable impairment of the glycolytic machinery at these higher concentrations. This could also account for the slight trend of SKOV3's to increase their respiratory rate upon incubation with 50 μg/mL (even though this increase is not statistically significant).

In conclusion, while the MMSN were well tolerated at the two incubation concentrations employed, any adverse effects that were registered, particularly at the highest incubation concentrations are cell-type dependent.

Preprints (www.preprints.org) | NOT PEER-REVIEWED | Posted: 23 October 2023 doi:10.20944/preprints202310.1429.v1

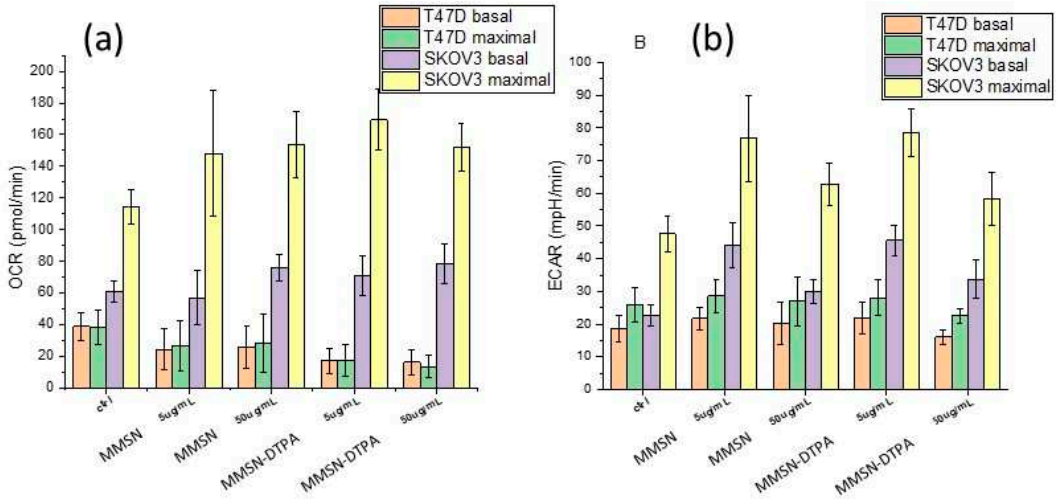

Figure 12. Metabolic measurements of MMSN and MMSN-DTPA incubated with T4TD and SKOV3 cells. Oxygen consumption rate measurement (a) and extracellular acidification rate measurement (b).

3. Materials and Methods

Materials Iron oxide (CAS 20344-49-4, Sigma Aldrich), oleic acid (CAS 112-80-1, Sigma Aldrich), *n*-docosane (CAS 629-97-0, Acros), oleylamine (CAS 112-90-3, Acros), tetraethyl orthosilicate TEOS (CAS 78-10-4, Sigma Aldrich), cetyltrimethylammonium bromide CTAB (CAS 57-09-0, Sigma Aldrich), pentane (CAS 109-66-0, Fisher), chloroform (CAS 67-66-3, Sigma Aldrich), trifluoroacetic acid (CAS 76-05-1, Fluorochem), triethylamine (CAS 121-44-8, Merck), dichloromethane (CAS 76-09-2, Carlo Erba), ethyl acetate (CAS 141-78-6, VWR), ethanol and acetone (Honeywell).

The *FTIR* spectra were recorded in the 4000-400 cm^{-1} range using 32 scans at a nominal resolution of 4 cm^{-1} using a Perkin Elmer 100 FT spectrophotometer equipped with an ATR unit. The ***TEM*** images were recorded with JEOL 1200 EXII microscope (JEOL Europe SAS, Croissy Sur Seine, France). For the purpose of TEM analysis, the sample particles were dispersed in ethanol and then deposited onto copper grids covered with porous carbon films. ***TGA analyses*** were performed with a thermal analyser STA 409 Luxx® (Netzsch) in the range 25-800 °C by a heating speed of 5 °C/min. DLS was performed with the use of a Cordouan Technologies DL 135 (Pessac). Zeta potentials were measured by a Malvern Nanoseries zetasizer, (Orsay), SEM-EDS technique was performed using a Flex-SEM 1000 II scanning electron microscope (Sweeden).

Metabolic assays, OCR and ECAR measurements, were performed on a Seahorse XFe96 Analyzer (Agilent Technologies, Santa Clara, CA).

Procedures

Synthesis of magnetic iron oxide nanoparticles (MIONs):

The MIONs were synthesized by thermal decomposition according to a previous reported protocol.[22] Briefly, 0.18 g of hydrated iron oxide (II) were mixed with 5 g of docosane and 3.2 g of oleic acid. The mixture was initially stirred under vacuum for 30 min and then placed under Ar flow for another 30 min. Then, the reaction occurred when heating at 340°C for 1h30. After completion of the reaction the MIONs were washed and recovered by three successive centrifugations at 20 krpm for 10 min and redispersion by ultrasound for a few minutes: 1) by adding 15 mL of pentane and 30 mL of a mixture of ether:ethanol (2:1, v:v) to the as-synthesized product, 2) by adding 2 mL of pentane and 30 mL of a mixture of ether:ethanol (2:1, v:v) to the collected black product, 3) by adding 30 mL of a mixture of ether:ethanol (1:1, v:v) to the collected black product. Finally the MIONs were stored in 15 mL of choloroform and stabilized by adding 200 µL of oleylamine.

 doi:10.20944/preprints202310.1429.v1

Synthesis of MMSN:

The scale-up protocol to synthesize 1 g of MMSN was designed by adapting a previous reported protocol that usually provided between 150-200 mg.[1] In the optimized process, 2 g of CTAB were first dissolved in 250 mL of distilled water for 1 h at 70°C under stirring in a 1 L flat and large bottom flask to enhance the liquid/air interface. The surfactant solution was then cooled down to 40°C and 5 mL from the previous synthesized MIONs dispersed in chloroform were added. The emulsion was first subjected to vigorous stirring without heating for 30 min and then the temperature was raised to 70°C for an additional 40 min of stirring to ensure the transfer of the MIONs from organic to aqueous phase. Once the phase transfer of MIONs succeeded, 300 mL of distilled water slightly basified by 300 µL of 2M NaOH were added to the solution under stirring. When the solution reached 60°C, 7.5 mL of TEOS followed by 12.5 mL of EtOAc were quickly added to the mixture. Then the condensation reaction was conducted for 3h at 70°C under stirring. The final MMSNs were recovered by centrifugation (5 to 10 min at 20 krpm), concentrated to 100 mL and washed two times: twice with water and twice with EtOH at 95 %. After each centrifugation step the MMSNs were redispersed in the appropriate washing solvent under sonication for few minutes. To extract the CTAB the MMSN were soaked twice in a solution of ammonium nitrate (6g/L in EtOH 90 %) and placed under stirring at 70°C for 2h. After each extraction, the washing steps by centrifugation described above in water and ethanol were performed.

Finally, the MMSN were redispersed in 25 mL of 96% EtOH.

Functionalisation of MMSN with DTPA:

In a typical procedure 2 mmol of DTPA per g of MMSN were added to a suspension of MMSN at 10 mg/mL in EtOH.

Briefly, 217 mg of diethylene triamine pentacetic anhydride, 135 mg of APTES and 61 mg of triethylamine were mixed in 40 mL of DMF under ultrasonds for 30 min. The mixture was then placed under stirring for 3h at room temperature. 30 mL of a suspension of MMSNs at 10 mg/mL in EtOH were then added. The solution was treated with ultrasound for 1h and then stirred at 80°C under reflux for 12 h. Finally the grafted nanoparticles, MMSN-DTPA, were washed by centrifugation once with EtOH, twice with water and once with acetone and then redispersed in EtOH.

Isotherm experiments of Ni2+, Co2+, Sm3+ and Nd3+ adsorption:

For isotherm experiments stock solutions of metal cations (50 mM) were prepared using nitrate salts and the final concentrations were adjusted by dilution with milli-q water (varying between 0.5-25 mM). Samples (10 mg) of magnetic nanoparticles (**MNPs**) were mixed with 10 mL of metal cation solution in plastic tubes of 50 mL and placed on a shaker for 24 hours. After each experiment, **MNPs** were centrifuged (7000 g) for 10 min and an aliquot (1 mL) was separated to determine the metal concentration in the remaining solution. The samples were first diluted 5-10 times (depending on the initial metal concentration) and titrated afterwards with EDTA using xylenol orange as an indicator. For each sample the titrations were repeated 3 times, and the average concentration was calculated.

The uptake of metal cation by the magnetic nanoparticles was calculated according to the equation:

$$Up=(C_o-C_e)*V/m$$

where: C_o is the initial metal concentration which was also measured by titration C_e is the equilibrium metal concentration V is the metal solution volume which was kept constant and m is the NPs weight.

For kinetic tests, the magnetic nanoadsorbents (20 mg) were mixed with 20 mL of metal cation solutions (with 10 mM initial metal concentration) and the uptake was measured after set time intervals. For that purpose, an aliquot of 1 mL was separated, diluted 10 times and the remaining metal concentration was evaluated by titration with EDTA and xylenol orange

For testing the selectivity, solutions of Ni:Nd, Co:Sm and Ni:Co in 1:1 ratio were used. 10 mg of adsorbent and 10 ml of test solutions in 50 mL plastic tubes were placed on a shaker for 24 hours. The particles were separated from metal solution by centrifugation (7000 g) and were dried under nitrogen atmosphere. They were subsequently analysed by SEM-EDS, to determine the metal ratios.

 doi:10.20944/preprints202310.1429.v1

Cell Culture:

Adult Human Dermal Fibroblasts (HDF) were purchased from Lifeline Cell Technology. Cells were maintained in RPMI medium supplemented with 10% fetal bovine serum (FBS) and penicillin/streptomycin. Cells were allowed to grow in a 5% CO_2 humidified atmosphere at 37 °C.

Cytotoxicity study:

Cells were seeded in 96-well plate at a density of 5000 cells *per* well. Twenty four hours after seeding, cells were treated with different concentrations (range from 0 to 250 µg mL^{-1}) of MMSN or MMSN-DTPA, and then cells were incubated for 72 h. After the incubation period, cells were processed for measuring their metabolic activity using the colorimetric MTT (3-(4,5-dimethylthiazolyl-2)-2, 5-diphenyltetrazolium bromide) assay. Accordingly, cells were incubated with MTT solution in culture medium at a concentration of 0.5 mg mL^{-1} for 4 h, then the medium was aspirated and the formazan crystals were dissolved using a mixture of DMSO/ethanol (1:1, v:v) with agitation for 20 min. The absorbance was read at 540 nm and the percentages of viable cells were calculated according to the following equation ($Ab_{test}/Ab_{control}$ *100). The experiments wwerer repeated 3 times. The dose-response curve was plotted as the log nanoparticles concentration in µg mL^{-1} versus the percentage of viable cells using GraphPad Prism 5.0 software (San Diego, CA, USA). The mean lethal concentration (LC_{50}) was determined at 50% of cell death.

Toxicity study in Zebrafish (Danio rerio) embryos:

Wild-type zebrafish embryos purchased from Zebrafish International Resource Center were used. These embryos were raised to adulthood in circulating aquarium system at 28 °C, 80% humidity, 14 h light/10 h dark cycle, in the lab's facilities of MMDN, Inserm U1198, Montpellier University, Montpellier. The day of the experiment, males and females were mated to produce fertilized embryos that were collected and maintained at 28°C. Five hours post fertilization (hpf), the embryos were examined under Loupe Olympus MVX10 stereomicroscope in order to choose the normally developed ones for the experiment. Embryos were placed in 12-well plate (20 embryos in each well) and exposed to 4 mL of water containing different concentrations (10, 25, 125 and 250 µg mL^{-1}) of MMSN or MMSN-DTPA. Mortality and viability (hatched or chorionated) were observed under the microscope at different time points that ended at 80 hpf. The statistical difference between the embryos death in control and tested groups was analysed by Student's t-test using GraphPad Prism 5.0 software (San Diego, CA, USA). The level of significance was defined as * $p < 0.05$, ** $p < 0.005$

Experiments with zebrafish embryos until 96 hpf are considered as *in vitro* studies according to the EU Directive 2010/63/EU on the protection of animals used for scientific purposes.[24]

Metabolic assay:

The metabolic profile of the iron oxide core, MMSN with and without DTPA, was studied in two human cell lines, SKOV3 ovarian adenocarcinoma and T47D breast ductal carcinoma. The cells were seeded in Agilent Seahorse XF96 cell culture 96-well plates at 30,000 cells per well and left overnight to attach in a humidified, 5% CO_2 atmosphere. Two cell groups were incubated for 4h with two concentrations of MMSN(±DTPA), 5 and 50 µg/mL respectively, while the control cells were kept in media. The 3 first hours of incubation were carried out in complete cell media and at a humidified 5% CO_2 atmosphere. During the last hour, however, the cells were incubated in unbuffered, seahorse, RPMI medium (pH 7.4) without FBS and in the absence of CO_2. Four basal oxygen consumption rate (OCR) and extracellular acidification rate (ECAR) were conducted in all cell groups, before the injection of 1µM Oligomycin A, an inhibitor of the F_0-F_1 ATPase. Three measurements were conducted following the injection to reveal the amount of OCR required for ATP synthesis. The second injection that followed was of 1 µM FCCP, a protonophore which uncouples the electron transport from oxidative phosphorylation, to show the maximal respiratory capacity. Following three measurements under the FCCP addition, the cells were injected with a cocktail of 1µM Rotenone and Antimycin A, specific inhibitors of the quinonereducing centres of complex I and III respectively. The

final three measurements under rotenone and Antimycin A, represent the background measurements of no mitochondrial respiration, since the two drugs completely inhibit electron transport.

4. Conclusions

The preparation of MMSN though thermal decomposition of FeO, was performed at the gram scale. The key parameters were the dispersion of the IO nanoparticles core, and the phase transfer procedure from $CHCl_3$ to water, which necessitated a larger neck glassware in order to properly evaporate $CHCl_3$. After functionalization with DTPA, The MMSN-DTPA were efficient in adsorbing Ni ions with a very good affinity and selectivity (with a ratio of 10) for Ni., compared to Co and Nd. Lower selectivity was noticed between Co and Sm where Sm was 2.4 times better adsorbed. Nanosafety of MMSN and MMSN-DTPA was examined in cells and a LC50 of 32 $\mu g.mL^{-1}$ was determined. No toxicity was noticed in the zebrafish model up to 125 $\mu g.mL^{-1}$. Metabolic experiments in cells showed that the MMSN and MMSN-DTPA are well tolerated.

Supplementary Materials: The following supporting information can be downloaded at the website of this paper posted on Preprints.org, Figure S1: Toxicological study of different concentrations of MMSN or MMSN-DTPA on zebrafish embryos development at different time points.

Author Contributions: For research articles with several authors, a short paragraph specifying their individual contributions must be provided. The following statements should be used "Conceptualization, G.S., J.-O.D., M.G.B., T.T. and L.R.; methodology, M.M., L.M.A.A.., A.V. and E.O.; validation, F.C., and A.B.; formal analysis, M.M., C.C., E.O.; writing—original draft preparation, M.M., J.-O.D.; writing—review and editing, M.M., T.T., G.S., L.M.A.A., J.-O.D., F.C., A.B.; supervision, C.C., L.R., G.S., J.O.D., M.G.B., All authors have read and agreed to the published version of the manuscript."

Funding: "This research was funded by ERA-MIN 2 MetRecycle project supported in Sweden by Vinnova grant No. 2018-00739. (2018-2021).

Institutional Review Board Statement: "Not applicable"

Informed Consent Statement: "Not applicable."

Data Availability Statement: Suggested Data Availability Statements are available in section "MDPI Research Data Policies" at https://www.mdpi.com/ethics.

Acknowledgments: In this section, you can acknowledge any support given which is not covered by the author contribution or funding sections. This may include administrative and technical support, or donations in kind (e.g., materials used for experiments).

Conflicts of Interest: "The authors declare no conflict of interest."

Sample Availability: Samples of the compounds are available from the authors.

References

1. Ménard, M.; Meyer, F.; Affolter-Zbaraszczuk, C.; Rabineau, M.; Adam, A.; Ramirez, P.D.; Bégin-Colin, S.; Mertz, D. Design of hybrid protein-coated magnetic core-mesoporous silica shell nanocomposites for MRI and drug release assessed in a 3D tumor cell model. *Nanotechnology* **2019**, *30*, 174001, doi:10.1088/1361-6528/aafe1c.
2. Gao, Q.; Xie, W.; Wang, Y.; Wang, D.; Guo, Z.; Gao, F.; Zhao, L.; Cai, Q. A theranostic nanocomposite system based on radial mesoporous silica hybridized with Fe3O4 nanoparticles for targeted magnetic field responsive chemotherapy of breast cancer. *RSC Adv.* **2018**, *8*, 4321-4328, doi:10.1039/C7RA12446E.
3. Das, R.K.; Pramanik, A.; Majhi, M.; Mohapatra, S. Magnetic Mesoporous Silica Gated with Doped Carbon Dot for Site-Specific Drug Delivery, Fluorescence, and MR Imaging. *Langmuir* **2018**, *34*, 5253-5262, doi:10.1021/acs.langmuir.7b04268.
4. Nasirzadeh, K.; Nazarian, S.; Hayat, S.M.G. Inorganic nanomaterials: a brief overview of the applications and developments in sensing and drug delivery. *J. Appl. Biotechnol. Rep.* **2016**, *3*, 395-402.
5. Wang, Y.; Zhou, B.; Wu, S.; Wang, K.; He, X. Colorimetric detection of hydrogen peroxide and glucose using the magnetic mesoporous silica nanoparticles. *Talanta* **2015**, *134*, 712-717, doi:10.1016/j.talanta.2014.12.013.

6. Wang, Y.; Li, B.; Zhang, L.; Li, P.; Wang, L.; Zhang, J. Multifunctional Magnetic Mesoporous Silica Nanocomposites with Improved Sensing Performance and Effective Removal Ability toward Hg(II). *Langmuir* **2012**, *28*, 1657-1662, doi:10.1021/la204494v.
7. Dib, S.; Boufatit, M.; Chelouaou, S.; Sadi-Hassaine, F.; Croissant, J.; Long, J.; Raehm, L.; Charnay, C.; Durand, J.O. Versatile heavy metals removal via magnetic mesoporous nanocontainers. *RSC Adv.* **2014**, *4*, 24838-24841, doi:10.1039/c4ra01323a.
8. Li, J.; Gong, A.; Li, F.; Qiu, L.; Zhang, W.; Gao, G.; Liu, Y.; Li, J. Synthesis and characterization of magnetic mesoporous Fe3O4@mSiO2–DODGA nanoparticles for adsorption of 16 rare earth elements. *RSC Adv.* **2018**, *8*, 39149-39161, doi:10.1039/C8RA07762B.
9. Mahdi, K.; Hamed, M.; Masoumeh, A.; Parham, S.-Z.; Michael, R.H. Smart mesoporous silica nanoparticles for controlled-release drug delivery. *Nanotechnology Reviews* **2016**, *5*, 195-207, doi:https://doi.org/10.1515/ntrev-2015-0057.
10. Knezevic, N.Z.; Gadjanski, I.; Durand, J.-O. Magnetic nanoarchitectures for cancer sensing, imaging and therapy. *J. Mater. Chem. B* **2019**, *7*, 9-23, doi:10.1039/c8tb02741b.
11. Liu, S.; Yu, B.; Wang, S.; Shen, Y.; Cong, H. Preparation, surface functionalization and application of Fe3O4 magnetic nanoparticles. *Adv. Colloid Interface Sci.* **2020**, *281*, 102165, doi:10.1016/j.cis.2020.102165.
12. Bagheri, E.; Ansari, L.; Abnous, K.; Taghdisi, S.M.; Naserifar, M.; Ramezani, M.; Alibolandi, M. Silica - magnetic inorganic hybrid nanomaterials as versatile sensing platform. *Nanomedicine Journal* **2020**, *7*, 183-193, doi:10.22038/nmj.2020.07.0002.
13. Gao, F. An Overview of Surface-Functionalized Magnetic Nanoparticles: Preparation and Application for Wastewater Treatment. *ChemistrySelect* **2019**, *4*, 6805-6811, doi:10.1002/slct.201900701.
14. Clemons, T.D.; Kerr, R.H.; Joos, A. Multifunctional magnetic nanoparticles: design, synthesis, and biomedical applications. In *Comprehensive Nanoscience and Nanotechnology (2nd Edition)*, Elsevier Ltd.: 2019; Vol. 3, pp. 193-210.
15. Albinali, K.E.; Zagho, M.M.; Deng, Y.; Elzatahry, A.A. A perspective on magnetic core-shell carriers for responsive and targeted drug delivery systems. *Int. J. Nanomed.* **2019**, *14*, 1707-1723, doi:10.2147/ijn.s193981.
16. Garcia, R.S.; Stafford, S.; Gun'ko, Y.K. Recent progress in synthesis and functionalization of multimodal fluorescent-magnetic nanoparticles for biological applications. *Appl. Sci.* **2018**, *8*, 172/171-172/123, doi:10.3390/app8020172.
17. Zhao, T.; Nguyen, N.-T.; Xie, Y.; Sun, X.; Li, Q.; Li, X. Inorganic Nanocrystals Functionalized Mesoporous Silica Nanoparticles: Fabrication and Enhanced Bio-applications. *Frontiers in Chemistry* **2017**, *5*, doi:10.3389/fchem.2017.00118.
18. Ling, D.; Lee, N.; Hyeon, T. Chemical Synthesis and Assembly of Uniformly Sized Iron Oxide Nanoparticles for Medical Applications. *Acc. Chem. Res.* **2015**, *48*, 1276-1285, doi:10.1021/acs.accounts.5b00038.
19. Knezevic, N.Z.; Ruiz-Hernandez, E.; Hennink, W.E.; Vallet-Regi, M. Magnetic mesoporous silica-based core/shell nanoparticles for biomedical applications. *RSC Adv.* **2013**, *3*, 9584-9593.
20. Liong, M.; Lu, J.; Kovochich, M.; Xia, T.; Ruehm, S.G.; Nel, A.E.; Tamanoi, F.; Zink, J.I. Multifunctional Inorganic Nanoparticles for Imaging, Targeting, and Drug Delivery. *ACS Nano* **2008**, *2*, 889-896.
21. Kim, J.; Kim, H.S.; Lee, N.; Kim, T.; Kim, H.; Yu, T.; Song, I.C.; Moon, W.K.; Hyeon, T. Multifunctional Uniform Nanoparticles Composed of a Magnetite Nanocrystal Core and a Mesoporous Silica Shell for Magnetic Resonance and Fluorescence Imaging and for Drug Delivery. *Angew. Chem. Int. Ed.* **2008**, *47*, 8438-8441, doi:10.1002/anie.200802469.
22. Nyalosaso, J.L.; Rascol, E.; Pisani, C.; Dorandeu, C.; Dumail, X.; Maynadier, M.; Gary-Bobo, M.; Kee Him, J.L.; Bron, P.; Garcia, M., et al. Synthesis, decoration, and cellular effects of magnetic mesoporous silica nanoparticles. *RSC Adv.* **2016**, *6*, 57275-57283, doi:10.1039/C6RA09017F.
23. Fan, H.; Leve, E.; Gabaldon, J.; Wright, A.; Haddad, R.E.; Brinker, C.J. Ordered Two- and Three-Dimensional Arrays Self-Assembled from Water-Soluble Nanocrystal–Micelles. *Adv. Mater.* **2005**, *17*, 2587-2590, doi:https://doi.org/10.1002/adma.200501088.
24. Seisenbaeva, G.A.; Ali, L.M.A.; Vardanyan, A.; Gary-Bobo, M.; Budnyak, T.M.; Kessler, V.G.; Durand, J.-O. Mesoporous silica adsorbents modified with amino polycarboxylate ligands – functional characteristics, health and environmental effects. *Journal of Hazardous Materials* **2021**, *406*, 124698, doi:https://doi.org/10.1016/j.jhazmat.2020.124698.